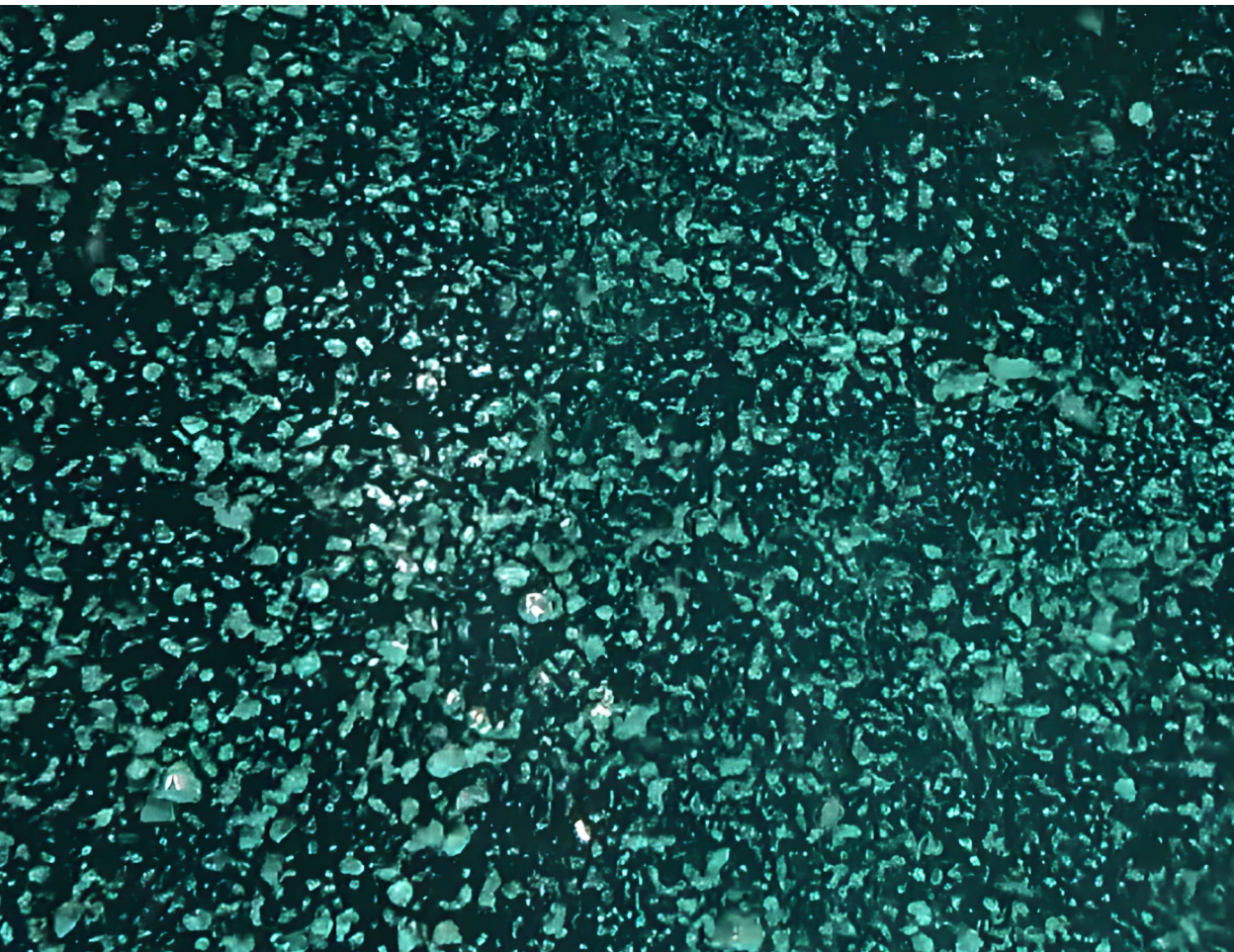


# Tracing methane sources and fate across the East Siberian Arctic Shelf using triple-isotopic analysis

Marenka Brussee





# Tracing methane sources and fate across the East Siberian Arctic Shelf using triple-isotopic analysis

Marenka Brussee

Academic dissertation for the Degree of Doctor of Philosophy in Environmental Sciences at Stockholm University to be publicly defended on Monday 25 May 2026 at 13.00 in Högbomsalen, Geovetenskapens hus, Svante Arrhenius väg 12 and online via Zoom, public link is available at the department website.

## Abstract

Atmospheric methane is rising rapidly due to a combination of anthropogenic and natural methane emissions. Uncertainties in the contributions of especially natural sources are high, while these emissions may alter in the near future due to climate change-induced feedback mechanisms. Permafrost regions are considered a natural source of methane, and thawing permafrost and associated greenhouse gas emissions represent a potential biogeochemical tipping point for climate change.

About one-seventh of the world's permafrost area is situated below sea level, predominantly on the East Siberian Arctic Shelf (ESAS). The ESAS sea region is the world's largest shelf sea system and was formed by sea level rise during the last deglaciation. This shelf seabed hosts large yet uncertain amounts of organic matter and methane in different deposits. While elevated methane concentrations have been observed in this region for more than two decades, the methane source and magnitude of methane emissions have been poorly constrained. Uncertainty in the methane sources limits the ability to estimate the magnitude of methane releases and expand these into future projections.

This PhD thesis focuses mainly on the knowledge gap on methane sources. The sedimentary drape contains fossil gas reservoirs, methane hydrates, preformed methane trapped by permafrost, and organic matter in frozen, thawed, and recently accumulated sediments that can be degraded to methane. The dual stable isotopic composition of methane ( $\delta^{13}\text{C}_{\text{CH}_4}$  and  $\delta^2\text{H}_{\text{CH}_4}$ ) is indicative of its formation pathway and potentiality of partial degradation. Methane's radiocarbon content constrains the age of the methane precursor. Therefore, triple-isotopic analyses of both seawater-dissolved and ebullitive methane were used to quantify the relative contributions of different methane sources to the observed elevated methane levels in both phases. To this end, a new preparation method for radiocarbon analysis of aqueous methane was developed. A second part of the thesis focuses on the fate of methane in both bubbles and seawater.

It was found that multiple methane sources contribute to the elevated methane concentrations across the ESAS, while at all hotspots, methane was dominantly old ( $^{14}\text{C}_{\text{age}} > 48000$  y before present). Microbial methane from subsea permafrost environments was the major methane source at methane hotspots in the inner Laptev Sea. In the East Siberian Sea and the outer Laptev Sea, fossil gas seeps of different origins were identified. The isotopic fingerprints of both dissolved and ebullitive methane in surface and bottom waters were similar and persistent over multiple years. In combination with concentration patterns, it was inferred that ebullition is an important source of methane to the water column. In the outer Laptev Sea, methane is oxidized in sub-pycnocline waters to measurable extents. In the inner Laptev Sea, no direct indication of strong methane oxidation was found. The high methane concentrations measured for surface bubbles ( $80 \pm 22\%$ ) show that methane is also directly transported from the seabed to the atmosphere. This ebullitive flux bypasses microbial degradation in both sediments and seawater. The implication of these results is that both ebullition and the multitude of methane sources across the ESAS need to be incorporated into future modeling efforts and included in methane release estimates for the ESAS region.

**Keywords:** *Methane, Subsea permafrost, Isotopic source apportionment, Radiocarbon, Arctic shelf sea, Carbon cycle, Climate change.*

Stockholm 2026  
<http://urn.kb.se/resolve?urn=urn:nbn:se:su:diva-254054>

ISBN 978-91-8107-586-1  
ISBN 978-91-8107-587-2

Department of Environmental Science

Stockholm University, 106 91 Stockholm





TRACING METHANE SOURCES AND FATE ACROSS THE EAST  
SIBERIAN ARCTIC SHELF USING TRIPLE-ISOTOPIC ANALYSIS

Marenka Brussee





# Tracing methane sources and fate across the East Siberian Arctic Shelf using triple- isotopic analysis

Marenka Brussee

©Marenka Brussee, Stockholm University 2026

ISBN print 978-91-8107-586-1

ISBN PDF 978-91-8107-587-8

Cover image: A screenshot of ebullitive methane filmed underwater during the International Siberian Shelf Study 2020 Expedition.

Printed in Sweden by Universitetservice US-AB, Stockholm 2026

To all cherishing  
creativity and our  
beautiful Earth



# Thesis Defense Committee

25 May 2026

## **Opponent**

Marcelo Ketzer, Professor at Linnaeus University

## **Members of the Grading Committee**

Gesa Weyhenmeyer, Professor at Uppsala University

Ruth Varner, Professor at University of New Hampshire

Joyanto Routh, Professor at Linköping University

## **Substitute Member of the Grading Committee**

Douglas Nilsson, Docent at Stockholm University

## **Chair for the Defense**

Johan Ström, Professor at Stockholm University



# Abstract

Atmospheric methane is rising rapidly due to a combination of anthropogenic and natural methane emissions. Uncertainties in the contributions of especially natural sources are high, while these emissions may alter in the near future due to climate change-induced feedback mechanisms. Permafrost regions are considered a natural source of methane, and thawing permafrost and associated greenhouse gas emissions represent a potential biogeochemical tipping point for climate change.

About one-seventh of the world's permafrost area is situated below sea level, predominantly on the East Siberian Arctic Shelf (ESAS). The ESAS sea region is the world's largest shelf sea system and was formed by sea level rise during the last deglaciation. This shelf seabed hosts large yet uncertain amounts of organic matter and methane in different deposits. While elevated methane concentrations have been observed in this region for more than two decades, the methane source and magnitude of methane emissions have been poorly constrained. Uncertainty in the methane sources limits the ability to estimate the magnitude of methane releases and expand these into future projections.

This PhD thesis focuses mainly on the knowledge gap on methane sources. The sedimentary drape contains fossil gas reservoirs, methane hydrates, preformed methane trapped by permafrost, and organic matter in frozen, thawed, and recently accumulated sediments that can be degraded to methane. The dual stable isotopic composition of methane ( $\delta^{13}\text{C}_{\text{CH}_4}$  and  $\delta^2\text{H}_{\text{CH}_4}$ ) is indicative of its formation pathway and potentially of partial degradation. Methane's radiocarbon content constrains the age of the methane precursor. Therefore, triple-isotopic analyses of both seawater-dissolved and ebullitive methane were used to quantify the relative contributions of different methane sources to the observed elevated methane levels in both phases. To this end, a new preparation method for radiocarbon analysis of aqueous methane was developed. A second part of the thesis focuses on the fate of methane in both bubbles and seawater.

It was found that multiple methane sources contribute to the elevated methane concentrations across the ESAS, while at all hotspots, methane was

dominantly old ( $^{14}\text{C}_{\text{age}} > 48000$  y before present). Microbial methane from subsea permafrost environments was the major methane source at methane hotspots in the inner Laptev Sea. In the East Siberian Sea and the outer Laptev Sea, fossil gas seeps of different origins were identified. The isotopic fingerprints of both dissolved and ebullitive methane in surface and bottom waters were similar and persistent over multiple years. In combination with concentration patterns, it was inferred that ebullition is an important source of methane to the water column. In the outer Laptev Sea, methane is oxidized in sub-pycnocline waters to measurable extents. In the inner Laptev Sea, no direct indication of strong methane oxidation was found. The high methane concentrations measured for surface bubbles ( $80 \pm 22\%$ ) show that methane is also directly transported from the seabed to the atmosphere. This ebullitive flux bypasses microbial degradation in both sediments and seawater. The implication of these results is that both ebullition and the multitude of methane sources across the ESAS need to be incorporated into future modeling efforts and included in methane release estimates for the ESAS region.

# Sammanfattning

Metanhalten i atmosfären ökar snabbt på grund av en kombination av antropogena och naturliga metanutsläpp. Osäkerheten kring bidraget från framför allt naturliga källor är stor, samtidigt som dessa utsläpp kan komma att förändras inom den nära framtiden till följd av feedbackmekanismer som orsakas av klimatförändringarna. Permafrostområden betraktas som en naturlig källa till metan, och utsläpp av växthusgaser från tinande permafrost representerar en potentiell biogeokemisk vändpunkt ("tipping point") för klimatförändringarna.

Cirka en sjundedel av världens permafrostområden ligger under havsnivån, främst på den östsibiriska arktiska kontinentalsockeln (ESAS). Havsområdet ESAS är världens största sockelhavssystem och bildades genom havsnivåhöjningen efter den senaste istiden. Denna kontinentalsockel rymmer stora men osäkert kvantifierade mängder organiskt material och metan i olika avlagringar. Trots att förhöjda metankoncentrationer har observerats i denna region i mer än två decennier, har metankällan och omfattningen av metanutsläppen varit svårt att fastställa. Osäkerheten kring metankällorna begränsar möjligheten att uppskatta storleken på metanutsläppen och utvidga dessa till framtida prognoser.

Denna doktorsavhandling fokuserar främst på kunskapsluckan kring metankällor. Sedimentlagren innehåller fossila gasreservoarer, metanhydrater, metan som fångats av permafrosten, samt organiskt material i frysta, tinade, och nyligen ackumulerade sediment som kan brytas ned till metan. Den stabila isotopsammansättningen av kol och väte i metan ( $\delta^{13}\text{C}_{\text{CH}_4}$  och  $\delta^2\text{H}_{\text{CH}_4}$ ) ger en indikation om dess bildningsprocess och eventuell partiell nedbrytning. Mätningar av kol-14-innehållet avgränsar åldern för ursprungsmaterialet. Därför användes dessa tre isotopmätningar för metan både löst i havsvatten, och som fri uppbyggande gas, för att identifiera vilka typer av källor som leder till de observerade förhöjda metanhalterna i båda faserna. För detta ändamål utvecklades en ny provpreparationsmetod för kol-14-analys av metan löst i vatten. En annan del av avhandlingen fokuserar på ödet för metan både som fria bubblor och som löst fas i havsvatten.

Det visade sig att flera metankällor bidrar till de förhöjda metankoncentrationerna i ESAS-regionen, medan metan vid alla hotspots

huvudsakligen var gammal ( $^{14}\text{C}$ -ålder > 48000 år före nutid). Mikrobiellt metan från permafrost under havsbotten var den huvudsakliga metankällan vid metanhotspots i den inre delen av Laptevhavet. I Östsibiriska havet och den yttre delen av Laptevhavet identifierades fossila gasläckor av olika ursprung. Isotopsignaturerna från både metan i lösning och bubblande metan i yt- och bottenvatten var lika och persistenta över flera år. I kombination med koncentrationsmönster drogs slutsatsen att bubblande metan är en viktig källa till metan i vattenpelaren. I det yttre Laptevhavet oxideras metan i vatten under pyknoklinen i mätbara omfattningar. I det inre Laptevhavet hittades inga direkta tecken på stark metanoxidation. De höga metankoncentrationerna som mättes för ytbubblor ( $80\pm 22\%$ ) visar att metan också transporteras direkt från havsbotten till atmosfären. Detta bubblande flöde kringgår mikrobiell nedbrytning i både sediment och havsvatten. Konsekvensen av dessa resultat är att både bubblandet och de många olika metankällorna i ESAS-regionen måste tas med i framtida modelleringsinsatser och inkluderas i uppskattningarna av metanutsläpp för ESAS-regionen.

# List of papers

The following papers are included in this thesis:

Paper I:

**M. Brussee**, H. Holmstrand, M. Süß, A. Davies, Ö. Gustafsson, Isolation of Methane from Ambient Water and Preparation for Source-Diagnostic Natural Abundance Radiocarbon Analysis. *Anal. Chem.* **96**, 17631–17639 (2024).

*Contributions: ÖG and HH initiated the project and contributed to the initial design, which was partially built and tested by HH, MS, and AD. MB continued this work and conducted additional experiments, resulting in several changes to the design and operating procedures. MB constructed and tested the final versions and operation procedures of the systems, performed all the overarching experiments reported in the article, and discussed these procedures, experiments, and results regularly with HH and ÖG. MB wrote the initial draft of the manuscript, including visualizations, which was circulated to all co-authors before submission.*

Paper II:

**M. Brussee**, H. Holmstrand, B. Wild, D. Kosmach, D. Chernykh, N. Shakhova, A. Kurilenko, I. Semiletov, Ö. Gustafsson, Triple-isotopic analyses pinpoint microbial methane release from subsea permafrost in the inner Laptev Sea. *Commun. Earth Environ.* **7** (2026).

*Contributions: The project to study methane release using triple-isotopic analysis was conceived and initiated by ÖG, HH, NS, and IS. Expeditions and methods to acquire sample material were organized and executed by ÖG, HH, BW, DK, DC, AK, and IS. MB directed the structuring of samples and data, ensured their long-term curation, and performed quality control on selected samples. MB and HH designed the preconcentration methods for dual stable isotope analysis. MB performed all isolations for radiocarbon analysis and did most stable isotope analyses. MB constructed the isotopic endmember database needed for isotopic source apportionment and*

regularly discussed these procedures with ÖG, BW, and HH. MB conducted all statistical analyses and wrote the initial draft of the manuscript, including the visualizations. The manuscript was mainly iterated with ÖG, BW, and HH, and thereafter with all co-authors.

Paper III:

**M. Brussee**, H. Holmstrand, B. Wild, D. Kosmach, D. Chernykh, A. Kurilenko, A. Salyuk, N. Shakhova, I. Semiletov, Ö. Gustafsson, Multiple subsea sources drive the extensive methane releases over the East Siberian Arctic Shelf. *Submitted to Science* (2026).

*Contributions: The division of tasks was very similar to Paper II. However, fewer meetings were held around this paper, as all methods and procedures were now established, and the isotopic endmembers were defined. MB measured the triple-isotopic composition of the majority of both ebullitive and dissolved methane samples and was responsible for the data handling of all methane data. Compared to Paper II less iterations of the manuscript were required until submission.*

Paper IV:

F. Yan, **M. Brussee**, H. Holmstrand, B. Wild, I. Semiletov, N. Shakhova, S. Kang, Ö. Gustafsson, Dual-stable isotope constraints on aerobic methane oxidation in the water column of the outer Laptev Sea. *Manuscript* (2026).

*Contributions: The initial idea to assess methane oxidation in the water column was conceived by ÖG, IS, and HH, and began as a pilot study using published data in a master's thesis project by Rosie Caldwell, who was supervised by MB, HH, and ÖG. Thereafter, FY and MB performed laboratory work to generate new stable isotope data for dissolved methane samples, and the interpretation methods were reevaluated. The data, methods, and interpretations were regularly discussed between FY, MB, HH, and ÖG. FY wrote the initial draft, including visualizations, which was circulated to all co-authors. MB gave detailed feedback in multiple iterations.*

# Contents

Abstract.....	i
Sammanfattning.....	iii
List of papers .....	v
1 Introduction .....	1
1.1 Rising methane levels from uncertain sources .....	1
1.2 Subsea permafrost, organic matter stocks, and methane deposits in the East Siberian Arctic Shelf region .....	1
1.3 Elevated methane concentrations in the East Siberian Arctic Shelf seawater .....	3
1.4 Unconstrained methane emissions on the East Siberian Arctic Shelf.....	4
1.5 Research objectives .....	6
2 Methods .....	7
2.1 Sample acquisition .....	7
2.2 Methane concentration analysis.....	7
2.3 Methane dual stable isotope analysis.....	8
2.4 Methane radiocarbon analysis.....	8
2.5 Isotopic endmembers.....	9
2.6 Bayesian Markov Chain Monte Carlo isotopic source apportionment .....	11
2.7 Assessment of aerobic methane oxidation.....	12
3 Results and Discussion .....	14
3.1 Developed preparation method for radiocarbon analysis of aqueous methane .....	14

3.2	Release of dominantly ancient methane on the ESAS .....	15
3.3	Multiple methane sources contribute to methane release in the ESAS region.....	17
3.3.1	Release of microbial methane from subsea permafrost environments in the inner Laptev Sea .....	17
3.3.2	Seepage of fossil gas in the outer Laptev Sea and East Siberian Sea.....	18
3.4	Aerobic methane oxidation in the water column .....	19
3.4.1	Inner Laptev Sea .....	19
3.4.2	Outer Laptev Sea .....	20
3.5	Ebullition represents an important transport vector for methane release.....	20
3.5.1	Ebullition: a source of methane to the water column .....	20
3.5.2	Ebullition: a transport pathway to the atmosphere .....	21
4	Conclusions and Outlook .....	22
5	References .....	24
	Acknowledgements.....	34

# 1 Introduction

## 1.1 Rising methane levels from uncertain sources

Methane ( $\text{CH}_4$ ) levels in the atmosphere are rising rapidly despite the urgency to reduce emissions<sup>1,2</sup>. As methane is the strongest contributor to global warming after carbon dioxide ( $\text{CO}_2$ ), having an 80 times higher global warming potential than  $\text{CO}_2$  over a period of 20 years, and a short lifetime of 9-12 years, reducing methane emissions rapidly could reduce effective radiative forcing on short time-scales effectively<sup>1-6</sup>. However, there exist large uncertainties in the relative and absolute contributions of diverse anthropogenic and natural methane emissions, alongside diverse unconstrained positive feedback mechanisms to climate change that increase natural methane emissions<sup>7-13</sup>.

One uncertainty in natural methane emissions is the contribution of methane release from permafrost systems<sup>14,15</sup>. As such release is partly driven by positive feedback mechanisms linked to global warming<sup>8,16-19</sup>, methane release from disturbed permafrost systems is considered a potential biogeochemical tipping point for climate change<sup>20</sup>. In conjunction with increasing atmospheric methane concentrations, a decrease in the carbon stable isotope values of methane ( $\delta^{13}\text{C}_{\text{CH}_4}$ ) is currently observed<sup>5,21-24</sup>. This shift can be explained by a combination of both changes in atmospheric and soil methane sinks and increased emissions of microbial methane that is depleted in  $^{13}\text{C}$ <sup>21,23-25</sup>. Microbial methane, having low  $\delta^{13}\text{C}_{\text{CH}_4}$  values, is also released from permafrost systems, yet its emission size is highly uncertain.

## 1.2 Subsea permafrost, organic matter stocks, and methane deposits in the East Siberian Arctic Shelf region

Permafrost is defined as subsurface material being at or below  $0^\circ\text{C}$  for at least two consecutive years<sup>26</sup>. It forms and grows during prolonged periods of cold climate<sup>27</sup>. Thick layers of permafrost were formed during the Pleistocene<sup>27,28</sup>. Currently, thick layers of permafrost are still present over large areas of the Arctic<sup>27,29,30</sup>. During the last deglaciation, starting after the Last Glacial

Maximum about 21000 years before present (BP), large permafrost areas got inundated, forming so-called subsea permafrost<sup>27,31,32</sup>.

The East Siberian Arctic Shelf (ESAS), the world's largest shelf sea, stretching up to 200 m depth  $\sim 1.7 \times 10^6$  km<sup>2</sup> with an average water depth of  $\sim 45$  m, contains about 60% of the world's subsea permafrost<sup>30,33</sup>. The extent of subsea permafrost underlying the ESAS shelf sea waters may be  $\sim 1.5 \times 10^6$  km<sup>2</sup> with an average thickness of  $\sim 330$  m<sup>30,31</sup>. The few existing measurements on changes in the subsea permafrost table (i.e., upper bound) measured 31-32 years apart, showed a thawing rate of  $\sim 14$  cm y<sup>-1</sup>, a rapid rate ( $\sim 35$  times faster) compared to its terrestrial counterpart<sup>34,35</sup>.

The ESAS region contains large organic matter (OM) and methane deposits. Organic matter is situated both in Holocene-accumulated sediments and in thawed/frozen subsea permafrost and can be degraded to methane under anoxic conditions<sup>16,34,36,37</sup>. While methane from OM may be produced below 0°C<sup>38-41</sup>, OM is especially prone to degradation upon thaw<sup>16,42,43</sup>. Preformed methane stocks from past OM degradation may be trapped within subsea permafrost<sup>38,41,44-47</sup>. Additional preformed methane deposits occur deeper in the seabed in fossil gas reservoirs from either microbial or thermogenic origin<sup>48-50</sup>. Such gases may, after formation, move to another reservoir below the subsea permafrost extent or get trapped below or within subsea permafrost<sup>47,48,51</sup>. Furthermore, any preformed methane trapped within or below the subsea permafrost extent may be partially present as methane hydrate if the required conditions of amount of methane, temperature, and pressure are met<sup>47,52-54</sup>.

The estimated amounts of carbon in OM and preformed methane deposits on the ESAS are highly uncertain. The amount of OM in Holocene sediments on the ESAS has been estimated as 23 GtC<sup>55</sup>. The amount of OM in subsea permafrost has been estimated as  $\sim 2800$  GtC for the circum-Arctic and  $\sim 500$  GtC for the ESAS specifically<sup>56,57</sup>. In comparison, the northern circumpolar terrestrial permafrost region, covering an area  $\sim 7$  times larger than the circum-Arctic subsea permafrost area, has been estimated to contain  $\sim 1400$ - $2000$  GtC in OM<sup>15,30,58,59</sup>. Preformed methane amounts associated with subsea permafrost and methane hydrates vary widely from 1 to 900 GtC for the ESAS region<sup>57,60</sup>. In comparison, the amount of methane stored in terrestrial permafrost hydrates, in an area  $\sim 9$  times larger than the ESAS subsea permafrost area<sup>30,61</sup>, has been estimated from 19 to 400 GtC<sup>60,62</sup>. Existing estimates of the amount of preformed methane in fossil gas resources for the ESAS region range from 1 to 5 GtC<sup>50,63,64</sup>. By comparison, terrestrial gas reserves and resources across Russia are estimated to contain  $\sim 100$  GtC of methane, i.e., 20-100 times more than the ESAS region, while having an area  $\sim 10$  times larger<sup>50,63-65</sup>. Despite all uncertainties in actual sizes, the OM and

methane deposits on the ESAS are large compared to the current amount of methane in the atmosphere, being  $\sim 4 \text{ GtC}^{20}$ .

### 1.3 Elevated methane concentrations in the East Siberian Arctic Shelf seawater

Elevated methane levels over large spatial scales of the ESAS, in addition to ebullition, have been observed for more than two decades<sup>57,66,67</sup>. Measured methane concentrations in the ESAS seawater were generally much larger than atmospheric equilibrium ( $\sim 4 \text{ nM}$ ). Figure 1 shows a compilation of circum-Arctic methane concentrations in surface waters ( $< 9 \text{ m}$  from the sea surface). It can be observed that methane concentrations are highest in areas underlain by subsea permafrost. This raises the question of whether methane release is associated with underlying subsea permafrost degradation.

Other coastal shelf systems worldwide also exhibit elevated methane concentrations<sup>66,68</sup>, and worldwide data show a strong inverse relationship between surface mixed-layer methane concentration and sea depth<sup>68</sup>. Yet, methane concentrations in the ESAS surface water appear to be higher than global surface mixed-layer data when comparing ESAS data to a global ocean methane data assembly<sup>68–70</sup>, i.e., by calculating the mean monthly disequilibrium (oversaturation) at a  $0.25^\circ$  horizontal resolution for the water column depth bins 0–50 and 50–200 m. For the depth range 0–50 m, the interquartile range of oversaturation for the worldwide data was 0.7–20  $\text{nM}^{68}$ , while 3–34  $\text{nM}$  for the ESAS (**Paper III**). For the depth range 50–200 m, the interquartile range of oversaturation for the worldwide data was 0.1–2  $\text{nM}^{68}$ , while 8–39  $\text{nM}$  for the ESAS (**Paper III**). Also, surface water concentration patterns are not directly related to sea depth on the ESAS but do show local methane hotspots (Figure 1 and **Paper II-III**).

Multiple aspects make the ESAS region special. In addition to the elevated methane concentrations, the spatial scale of this shelf sea is very large, as the shelf sea coast stretches about 2500 km wide, with the shelf edge 400–800 km from the modern coastline<sup>31,71</sup>. The history of the ESAS region is also unique in not being glaciated during the Last Glacial Maximum, unlike many other northern shelf sea regions<sup>72–74</sup> facilitating the existence of subsea permafrost today<sup>30,31</sup>. Furthermore, global submarine seepage is dominated by the ESAS region, and its emissions represent the main uncertainty and control on the size of global submarine seepage<sup>75</sup>. Importantly, the high methane concentrations observed in the ESAS surface water (Figure 1) suggest that the ESAS region is a net methane source.

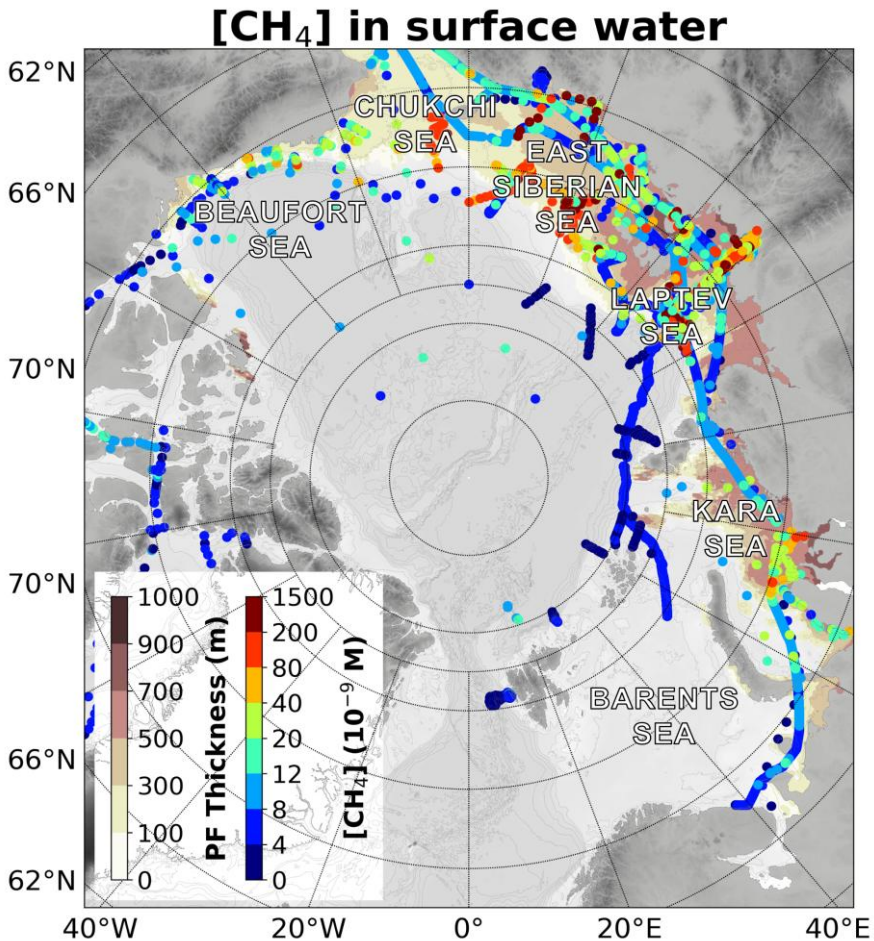


Figure 1: A compilation of circum-Arctic surface water methane concentrations (< 9 m below sea level): published data<sup>66,76–90</sup> and data in submission (**Paper III**). In the background, the modeled circum-Arctic subsea permafrost (PF) thickness<sup>30</sup> is shown.

#### 1.4 Unconstrained methane emissions on the East Siberian Arctic Shelf

Estimated methane fluxes from the ESAS region vary widely. Existing estimates using different methods range from 3 to 17 Tg CH<sub>4</sub> y<sup>-1</sup><sup>66,67,86,91</sup>. In comparison, estimated methane fluxes for the northern Arctic and boreal terrestrial permafrost region, including wetlands and lakes, which is ~11 times larger than the ESAS region, have been estimated at 20–51 Tg CH<sub>4</sub> y<sup>-1</sup><sup>15</sup>. Despite a substantial methane flux from the ESAS region, methane release

from subsea permafrost is currently excluded from Arctic carbon and global methane budgets<sup>7,92</sup>.

The Arctic is warming rapidly at a rate three to four times the global average<sup>93,94</sup>. Arctic warming results in several unconstrained carbon-climate feedbacks, among them the potential for increased methane emissions from the ESAS region. In addition, both methane release from dissociating methane hydrates and thawing permafrost are considered potential biogeochemical tipping points for climate change<sup>20</sup>.

Methane emissions from the ESAS region can increase through different feedback mechanisms. Firstly, warming of the Arctic and of seawater, as observed in bottom water of the Laptev Sea<sup>67,95</sup>, may lead to thawing of subsea permafrost and increased degradation rates of OM in (thawed) sediments. Lateral inputs of OM and methane might increase due to increased coastal erosion, increased terrestrial permafrost degradation, and associated river export<sup>96–99</sup>. In addition to these mechanisms, increasing seabed temperatures may lead to dissociation of methane hydrates, releasing preformed methane while facilitating additional upward transport of formerly trapped methane. The destabilization of the subsea permafrost environment itself may also result in direct release of preformed methane by methane escaping from methane pools originally trapped by the subsea permafrost layer. Preformed methane from fossil gas reservoirs at greater depth may also seep upwards along tectonic faults<sup>48,49,100</sup>. Global warming and non-tectonic processes, such as changes in ocean loading, are suggested to influence seismic activity in coastal regions<sup>101–103</sup>. All these mechanisms together suggest that methane release from the ESAS is unlikely to decrease; rather, it is likely to increase.

A major knowledge gap for estimating methane release sizes using modeling approaches is the lack of understanding of which methane source contributes to the observed methane release on the ESAS. As each methane source responds differently to global warming, as described above, knowing the relative and absolute contributions from each source is crucial for predicting methane release trajectories for the ESAS region. In addition to understanding methane sources, it is crucial to know which fraction of methane is transported to the atmosphere via the dissolved phase or ebullition. For the dissolved transport vector, it is furthermore important to know how much methane is removed by microbial oxidation while being in the dissolved phase. Lacking knowledge of methane sources, transport pathways, and microbial degradation limits the ability to predict future ESAS methane emissions in a further-warming climate. The overarching goal of this thesis is to constrain the relative contributions of the dominant methane sources at methane hotspots in the ESAS region.

## 1.5 Research objectives

Multiple research objectives are covered in this thesis, along with the primary goal of constraining methane sources in the ESAS region:

- 1. Develop a preparation method for radiocarbon analysis of aqueous methane (Paper I).**

In this PhD project, triple-isotopic methane data were generated and used for source apportionment of released methane in the ESAS region. This required a method that allowed measuring the radiocarbon content of methane in aqueous samples. Therefore, the first objective was to develop this method.

- 2. Constrain the dominant methane sources at different methane hotspots across the ESAS (Paper II-III).**

Three major methane hotspots on the ESAS were identified. For each of these methane hotspots, the dominant methane sources to the elevated levels were constrained using triple-isotopic methane data, isotopic endmembers, and a Bayesian statistical framework. The three major methane hotspots were located in the inner Laptev Sea, outer Laptev Sea, and East Siberian Sea. Objective 2 contains the following subobjectives:

- A.** Define potential endmembers for methane source apportionment in the ESAS region and construct an isotopic endmember database that allows quantification of the relative contribution of different methane sources to the observed elevated methane (**Paper II**).

- B.** Quantify the relative source contributions to both ebullitive and seawater dissolved methane to identify the dominant methane sources in both phases (**Paper II** and **Paper III**).

- 3. Characterize the fate of methane after release from the seabed (Paper II-IV).**

To investigate the fate of methane after release from the seabed, the dual stable isotopic composition of methane was followed along the water column, and dual-phase methane was analyzed for both concentration and triple-isotopic composition in both surface and bottom water. With these data, bubble dissolution (**Paper III**), methane oxidation in the water column (**Paper II** and **Paper IV**), and methane transfer to the atmosphere (**Paper II** and **Paper III**) were described.

## 2 Methods

### 2.1 Sample acquisition

Five expeditions to the East Siberian Arctic Shelf were conducted between 2014 and 2020, yielding methane samples used in this PhD project. The Swedish icebreaker Oden traversed the outer parts of the Laptev Sea and East Siberian Sea in 2014. The R/V Akademik M.A. Lavrentyev crossed the inner and outer Laptev Sea and the East Siberian Sea in 2016. In 2018-2020, the R/V Akademik Mstislav Keldysh transited the inner and outer Laptev Sea in 2018 and all studied seas (inner and outer Laptev Sea and East Siberian Sea) in 2019 and 2020.

Using the echosounders *Simrad EK60* in 2014 and the *Simrad EK15* in 2016-2020, bubble flares were identified. Seawater samples were collected at stations along the ship tracks, with intensified sampling for isotopic analysis of methane in regions near locations where such bubble flares were identified and/or strongly elevated methane concentrations were observed.

Seawater was collected using different methods. Most seawater samples were collected using Niskin sampling flasks on a Niskin Rosette that had a CTD (Conductivity, Temperature, Depth) probe. Further samples were collected using a seawater intake system (2.5 and 8 m deep) and from the overlying seawater of sediments obtained with an *Oktopus* multicorer. Gas bubble samples were collected using an inverted bottle on a cone-shaped bubble trap<sup>104</sup>. Details regarding all sampling procedures are in **Paper II** and **Paper III**.

### 2.2 Methane concentration analysis

Dissolved methane concentrations were measured onboard using gas chromatography flame ionization detection (GC-FID). Seawater was equilibrated with helium gas in plastic 60 mL syringes by active shaking, followed by resting, and the equilibrated headspace gas was thereafter extracted for subsequent injection into the GC-FID. Three to five calibration standards ranging from 1.63 to 1067 ppm were used for calibrating signal intensity versus methane concentration. Details are in **Paper II** and **Paper III**.

Bubble gas samples were analyzed onboard for methane and ethane concentrations using GC-FID. For each expedition, one calibration standard (83/85% methane, 187/209 ppm ethane) was used, and the calibration curve was forced through the origin. Details are in **Paper III**.

## 2.3 Methane dual stable isotope analysis

The dual stable isotopic composition of the dissolved and bubble methane samples ( $\delta^{13}\text{C}_{\text{CH}_4}$  and  $\delta^2\text{H}_{\text{CH}_4}$ ) was measured at Stockholm University by using gas chromatography continuous-flow isotope ratio mass spectrometry (GC-CF-IRMS). Bubble gas showed such high methane concentrations that bubble gas could be injected directly into the injection port, leading to the GC column. For calibration, one methane standard (99.99% methane) was used. Details are in **Paper III**.

Seawater-dissolved methane was first equilibrated into helium gas before stable isotope analysis of methane was performed. A helium gas headspace was introduced into the samples (serum bottles containing seawater), which were then shaken and subsequently allowed to rest for equilibration. This resulted in gas headspaces with relatively low methane concentrations in helium. Therefore, direct injection was not possible, and methane preconcentration was required. A preconcentration procedure, similar to Rice et al. (2001)<sup>105</sup>, was used for this, but with minor modifications. Firstly, all traps were cooled to lower temperatures by immersing the traps in liquid nitrogen ( $\text{LN}_2$ ) during the cooling stages. Furthermore, a dry-ice cooled PoraPLOT Q column was added after the third trap to separate methane from traces of  $\text{N}_2$  and  $\text{O}_2$ . Thereafter, an additional cryofocusing stage was added to re-concentrate the methane before injection into the GC column. This fourth trap also contained a PoraPLOT Q column and was cooled with  $\text{LN}_2$ . For calibration, two methane standards of 1.85 ppm methane in synthetic air of different isotopic composition were used. Details are in **Paper II** and **Paper III**.

## 2.4 Methane radiocarbon analysis

The natural abundance radiocarbon signal of ebullitive and dissolved methane ( $\Delta^{14}\text{C}_{\text{CH}_4}$ ) was measured using accelerator mass spectrometry (AMS) at the Tandem Laboratory in Uppsala (Faculty of Science and Technology, Uppsala University). Ebullitive methane had such high methane concentrations that no elaborate preparation procedures were required. The ebullitive methane was subsampled into glass vials, which were as preparation cleaned with helium gas and thereafter filled with helium gas. This resulted in an

overpressure in the glass vials. The content of these glass vials was consequently extracted at the Tandem Laboratory and combusted to CO<sub>2</sub> before graphitization and analysis by AMS.

For dissolved methane samples, an analytical challenge was present. Seawater samples contain trace amounts of dissolved methane next to extensive amounts of other carbon-containing gases. Therefore, methane needed to be extracted from seawater and purified from other carbon-containing gases before combustion of the extracted and purified methane to CO<sub>2</sub>, with the resulting CO<sub>2</sub> subsequently analyzed by AMS. A new analytical method was developed for methane extraction, purification, and conversion to CO<sub>2</sub>, as further described in section 3.1. This method enabled compound-specific natural abundance radiocarbon analysis of aqueous methane.

## 2.5 Isotopic endmembers

Triple-isotopic data of ebullitive and seawater-dissolved methane ( $\Delta^{14}\text{C}_{\text{CH}_4}$ ,  $\delta^{13}\text{C}_{\text{CH}_4}$ ,  $\delta^2\text{H}_{\text{CH}}$ ) were generated to constrain the methane source. In order to apply isotopic source apportionment, the potential methane sources (endmembers) and their isotopic compositions were defined. Because the radiocarbon data pointed to a dominant radiocarbon-free methane source (section 3.2), only old sources ( $^{14}\text{C}_{\text{age}} > 48000$  y BP) were considered. Three old methane sources were defined and isotopically constrained, as detailed in **Paper II**. These three constrained endmembers are also visualized in the situation sketch showing potential methane sources in the ESAS region (Figure 2).

In short, the first two endmembers were two different types of fossil gas: fossil thermogenic and secondary microbial (FOTSEM) gas and fossil primary microbial (FOPRIM) gas. These two types of fossil gas differ in their formation depths and temperatures and exhibit distinct dual stable isotopic compositions. These isotopic endmembers were primarily constrained using a global dataset of fossil gas data<sup>21,106</sup> limited to the regions: Russia, Kazakhstan, Europe, Canada, Alaska, China, and Japan. From this global subset, isotopic data of the two defined types of fossil gas were extracted using methane to ethane and propane ratios,  $\delta^{13}\text{C}_{\text{CO}_2}$  values, and definitions by Milkov & Etiope (2018)<sup>107</sup>. Following similar selection procedures and definitions, additional samples found in the literature were added to the endmember database.

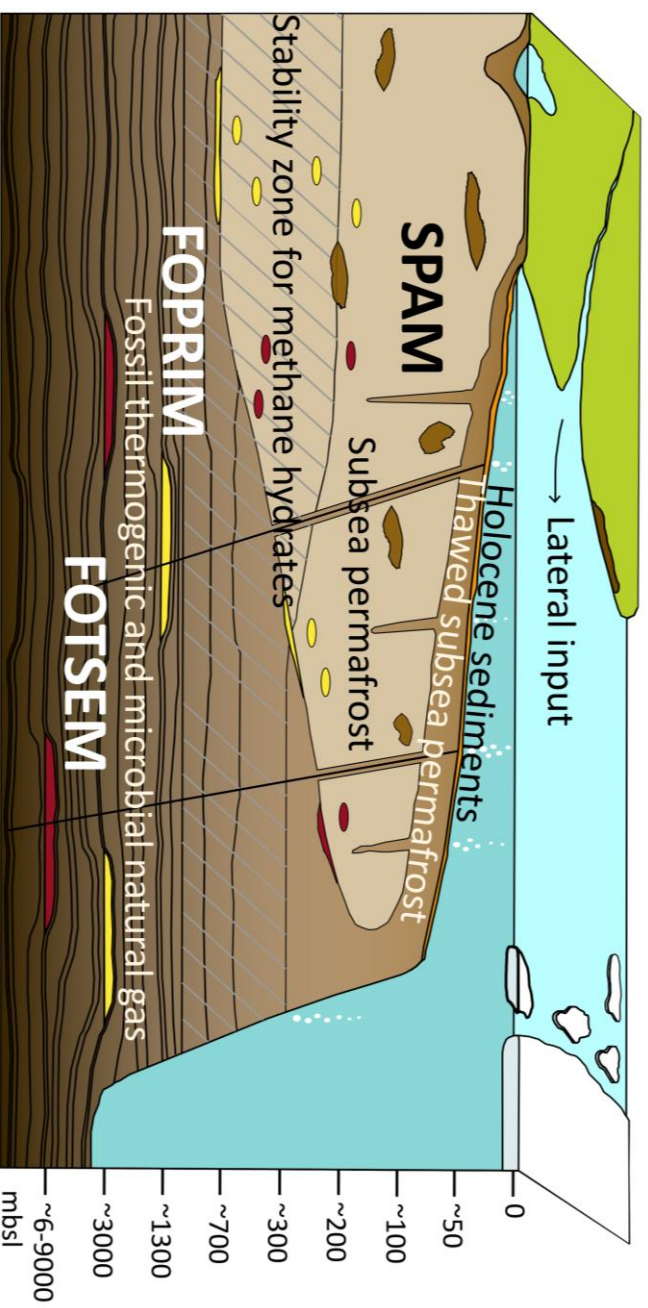


Figure 2: Situation sketch showing potential methane sources in the East Siberian Arctic Shelf region and the three constrained old ( $^{14}\text{C}_{\text{age}} > 48000 \text{ y BP}$ ) endmembers: fossil thermogenic and secondary microbial (FOTSEM) gas (indicated in red), fossil primary microbial (FOPRIM) gas (indicated in yellow), and subsea permafrost-associated methane (SPAM). The depth range is indicated with approximate depths in meters below sea level (mbsl). This situation sketch is adapted from **Paper II**.

The third endmember was subsea permafrost-associated methane (SPAM). This endmember represents methane that is formed upon thawing or before/during freezing of the subsea permafrost layer. This endmember was constrained using isotopic data on preformed methane in Northern Hemisphere permafrost and on methane in gas bubbles released from lakes in Northern Hemisphere permafrost regions. Both procedures yielded similar isotopic endmember values, and the average of these two procedures was used to define the isotopic composition of the endmember SPAM.

## 2.6 Bayesian Markov Chain Monte Carlo isotopic source apportionment

The generated methane isotope data were combined with the constrained endmembers in a Bayesian statistical framework to calculate the relative contribution of each identified source to the observed elevated methane. The statistical framework was, to a large extent, similar to one described previously<sup>108,109</sup> but with minor alterations in the iterative scheme.

The observed elevated methane was considered a combination of methane released from three sources as defined in section 2.5. Therefore, the measured isotopic source signatures were related to the isotopic compositions of the endmembers using the following set of linear equations:

$$\delta^{13}C_s = f_{SPAM}\delta^{13}C_{SPAM} + f_{FOPRIM}\delta^{13}C_{FOPRIM} + f_{FOTSEM}\delta^{13}C_{FOTSEM}$$

$$\delta^2H_s = f_{SPAM}\delta^2H_{SPAM} + f_{FOPRIM}\delta^2H_{FOPRIM} + f_{FOTSEM}\delta^2H_{FOTSEM}$$

$$1 = f_{SPAM} + f_{FOPRIM} + f_{FOTSEM}$$

(equation 1),

where  $\delta^{13}C_s$  and  $\delta^2H_s$  are the sample-derived isotopic source signatures,  $\delta^{13}C_{SPAM}, \dots, \delta^2H_{FOTSEM}$  the isotopic compositions of the endmembers and  $f_{SPAM}, f_{FOPRIM}, f_{FOTSEM}$  the unknown fractional source contributions.

Because the endmembers have an uncertainty in their isotopic composition, calculating the analytical solution for the fractional source contributions and their associated uncertainties is extremely complicated. Therefore, a Bayesian Markov Chain Monte Carlo (MCMC) algorithm was used to draw samples from the probability distributions of the unknown fractional source contributions ( $f_{SPAM}, f_{FOPRIM}, f_{FOTSEM}$ ) and, by doing so, retrieve the probability density functions of these fractions. The selected algorithm to sample from the unknown probability density function  $p(f_{SPAM}, f_{FOPRIM}, f_{FOTSEM} | \delta^{13}C_s, \delta^2H_s)$  was the Metropolis-Hastings algorithm

with symmetric transition probability, i.e., the symmetric random walk Metropolis algorithm<sup>110</sup>.

The transition function in the algorithm was defined as follows:

$$\begin{pmatrix} f_{SPAM_{n+1}} \\ f_{FOPRIM_{n+1}} \\ f_{FOTSEM_{n+1}} \end{pmatrix} = \begin{pmatrix} f_{SPAM_n} \\ f_{FOPRIM_n} \\ f_{FOTSEM_n} \end{pmatrix} + h\beta \begin{pmatrix} 1 \\ -1 \\ 0 \end{pmatrix} + h\gamma \begin{pmatrix} 0 \\ 1 \\ -1 \end{pmatrix} \quad (\text{equation 2}),$$

where  $h$  is a constant value and  $\beta, \gamma \sim N(0,1)$ . Therefore, the transition probability is symmetric. If, in an iteration, a fractional source contribution became less than 0, the fractional source contributions were set equal to those of the former iteration. The stochastic perturbation value  $h$  was chosen such that the accepted fraction of iterations was close to 0.23, which is an optimal fraction of acceptance<sup>111</sup>.

In the iterative scheme, the acceptance probability was calculated as follows:

$$\alpha = \min \left\{ \frac{p(\delta^{13}C_s | f_{SPAM_{n+1}}, f_{FOPRIM_{n+1}}, f_{FOTSEM_{n+1}})}{p(\delta^{13}C_s | f_{SPAM_n}, f_{FOPRIM_n}, f_{FOTSEM_n})} \cdot \frac{p(\delta^2H_s | f_{SPAM_{n+1}}, f_{FOPRIM_{n+1}}, f_{FOTSEM_{n+1}})}{p(\delta^2H_s | f_{SPAM_n}, f_{FOPRIM_n}, f_{FOTSEM_n})}, 1 \right\} \quad (\text{equation 3}).$$

The fractional source contributions of the next iteration ( $f_{SPAM_{n+1}}, f_{FOPRIM_{n+1}}, f_{FOTSEM_{n+1}}$ ) were accepted when  $\alpha \geq u$ , where  $u \sim U(0,1)$ . When  $\alpha < u$ , the fractional source contributions were set equal to those of the former iteration. For initialization, all source fractions were set equal to 1/3. The implementation of this algorithm is detailed in **Paper II**.

## 2.7 Assessment of aerobic methane oxidation

Aerobic methane oxidation was quantitatively assessed in the outer Laptev Sea. The dual stable isotopic composition of a methane pool changes during aerobic methane oxidation because methane isotopologues react at different rates. For a closed well-mixed system, the  $\delta^{13}C_{CH_4}$  and  $\delta^2H_{CH_4}$  values of the remaining methane are expected to increase with reducing methane concentrations upon aerobic methane oxidation according to the Rayleigh equation (e.g., Criss (1995)<sup>112</sup>, Li et al. (2024)<sup>113</sup>):

$$\ln \left( \frac{\delta X + 1000}{\delta X_0 + 1000} \right) = (\alpha_X - 1) \ln \left( \frac{C}{C_0} \right) \quad (\text{equation 4}).$$

In equation 4,  $\delta X_0$  represents the original stable carbon/hydrogen isotope value of methane before oxidation and  $C_0$  the associated methane concentration. Furthermore,  $\delta X$  represents the stable carbon/hydrogen isotope value of the remaining methane when the original methane pool is partly oxidized, such that the concentration has reduced from  $C_0$  to  $C$ . Lastly,  $\alpha_X$  represents the fractionation factor of either carbon or hydrogen. In **Paper IV**, the inverse of  $\alpha$ , i.e., the kinetic isotope effect (KIE) is used in all calculations, and equations 4 and 5 are adapted accordingly.

Although seawater in the ESAS region does not mimic a closed system, water parcels are assumed to be such in **Paper IV**. In this study, it was assumed that dissolved methane in seawater was oxidized during transport, i.e., a Lagrangian approach similar to Leonte et al. (2017)<sup>14</sup>. For each station, it was first tested whether the samples showed a Rayleigh-type behavior, i.e., whether  $\ln(C)$  was inversely proportional to  $\ln(\delta X + 1000)$ . In case the samples of a specific station showed such a relationship, for each sample, the fraction oxidized ( $f_{ox}$ ) was calculated using equation 5, which is derived from equation 4:

$$f_{ox} = 1 - \left( \frac{\delta X + 1000}{\delta X_0 + 1000} \right)^{\frac{1}{\alpha_X - 1}} \quad (\text{equation 5}).$$

In equation 5, the starting stable carbon/hydrogen isotope value  $\delta X_0$  was inserted as the mean stable carbon/hydrogen isotope value of the highest-concentration dissolved methane samples and the lowest stable carbon/hydrogen isotope values measured at that specific station.

## 3 Results and Discussion

### 3.1 Developed preparation method for radiocarbon analysis of aqueous methane

A new preparation method for radiocarbon analysis of aqueous methane was developed as part of research objective 1. Existing methods for compound-specific radiocarbon analysis of dissolved methane were not suitable for the intended purpose of this study. Some existing methods were not proven/developed for low-concentration samples<sup>84,115,116</sup> while another method had such extensive sampling times<sup>117</sup> that limit sampling coverage during expeditions. Furthermore, the removal of carbon monoxide (CO)<sup>115,116</sup> and nonmethane hydrocarbons (NMHCs)<sup>116</sup> was not demonstrated for all existing methods, while such removal is crucial for seawater-dissolved methane analysis, where such molecules are present. Additionally, the total processing blanks of all existing methods were either high (5  $\mu\text{g C}$  or larger) or not reported at all<sup>84,115–118</sup>, limiting analysis of low-concentration samples. Furthermore, the  $\Delta^{14}\text{C}_{\text{CH}_4}$  value of the total processing blank was not determined for most existing methods<sup>84,115–117</sup>. The analytical protocol developed here addresses and overcomes the limitations of previous approaches.

The complete description and all test results of the newly developed preparation method for radiocarbon analysis of aqueous methane are presented in **Paper I**. The method consists of two parts. The first part is an optionally field-operated system for extracting methane from ambient water and prepurifying it by largely removing water vapor and  $\text{CO}_2$ : the  $\text{CH}_4$  Stripping and Purification System (STRIPS). The second system is the  $\text{CH}_4$  Isotope Preparation System (CHIPS), which further purifies the STRIPS-isolated sample by removing residual non-methane carbon and then oxidizes the purified methane to  $\text{CO}_2$  for subsequent AMS analysis.

Challenges in developing such a preparation method for compound-specific radiocarbon analysis of aqueous methane include the amount of aqueous sample material required and the extraction and purification of methane from it without introducing any ambient carbon-containing gases. The collaborating laboratory offering AMS analysis posed the requirements for the final product of the sample preparation method. The required sample format was: pure  $\text{CO}_2$  with a minimum carbon amount of 10  $\mu\text{g C}$ .

The chosen sample volume was 30 L of water so that the method would work down to 40 nM. Furthermore, to reduce uncertainty in the methane radiocarbon data, the amount of non-methane-derived CO<sub>2</sub> in the final sample product, i.e., the total processing blank, should be small and have as low an uncertainty as possible. In the design of **Paper I**, this carbon blank ( $\pm 2\sigma$ ) was smaller than 1  $\mu\text{g C}$ , which is lower than the total processing blank of any known published preparation method for radiocarbon analysis of aqueous methane samples.

The low carbon blank was acquired due to several design aspects. One important aspect was to operate at overpressure in both systems of the preparation method to minimize direct gas leakage into the system as much as possible. While working at high pressure has been considered a risk when using a gas line that includes oxygen and that is cooled with liquid nitrogen, the developed method is operated at such low oxygen partial pressures that, as long as all procedures are strictly followed, there is no risk of liquid oxygen formation. A second important aspect was the guidance of gas through the second system, CHIPS. It was decided to design the system as operator-heavy, with the gas route altering during many time-specific steps. This has reduced the carbon blank enormously, as blank-increasing steps could be bypassed as much as possible, and only parts of the gas line were included when a specific processing step was needed.

A practical feature of the design is that the first system, STRIPS, can be employed in the field, and only small intermediate sample containers need to be transported to an on-site laboratory facility having the second system, CHIPS. Storage capacity in these intermediate small-sample containers was tested for up to 323 days without any decrease in methane recovery. The developed analytical protocol was used to generate all aqueous methane radiocarbon data for this PhD thesis.

### 3.2 Release of dominantly ancient methane on the ESAS

All generated radiocarbon data of both dissolved and bubble methane samples retrieved across the East Siberian Arctic Shelf pointed to the release of dominantly ancient methane ( $\Delta^{14}\text{C}_{\text{CH}_4} < -998\text{‰}$ ,  $^{14}\text{C}_{\text{age}} > 48000$  y BP) at all methane hotspots (**Paper II** and **Paper III**). While a younger methane background was observed at lower methane concentrations in the inner Laptev Sea and the East Siberian Sea, which likely indicated microbial methane production in younger sediment, the dominant methane source was old (Figure 3). This implies that methane observed at methane hotspots predominantly originates from deep preformed methane pools or from organic matter in subsea permafrost with a  $^{14}\text{C}_{\text{age}} > 48000$  y BP.

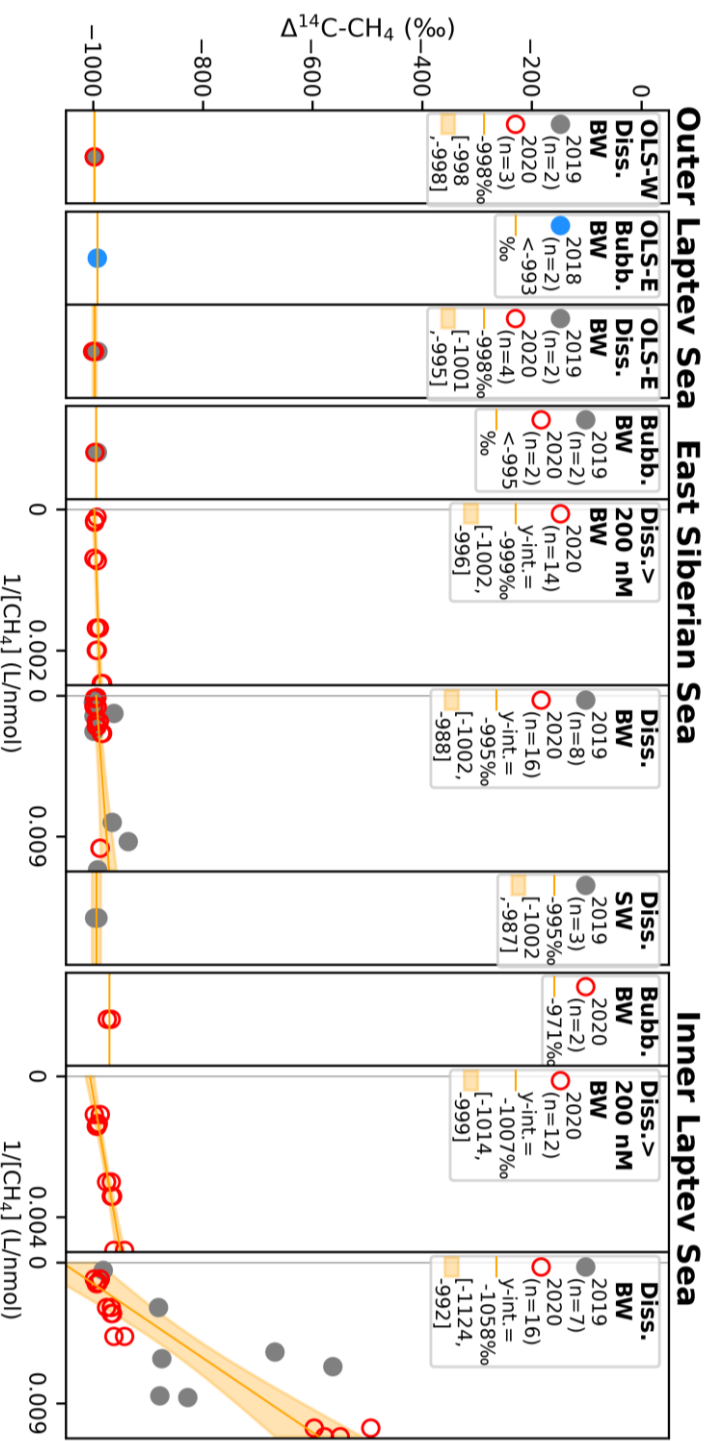


Figure 3: All methane radiocarbon data ( $n=69$ ) generated as part of this PhD thesis. The figure is adapted from **Paper II** and **Paper III**. The radiocarbon content of both dissolved (Diss.) and bubble (Bubb.) methane was measured in both bottom water (BW) and surface water (SW) samples for different years. For dissolved samples shown with Keeling plots, the Keeling plot y-intercept (y-int.) and its 95% confidence interval of this isotopic source signature are shown in the legend. For ebullitive samples and dissolved samples with no variation in  $\Delta^{14}\text{C}_{\text{CH}_4}$  with methane concentration, the mean  $\Delta^{14}\text{C}_{\text{CH}_4}$  values and associated 95% confidence intervals are shown as orange horizontal lines and shaded areas, and are reported in the legend.

As the observed elevated methane in both phases was dominantly radiocarbon-free, the three endmembers for the source apportionment were: fossil thermogenic and secondary microbial (FOTSEM) gas, fossil primary microbial (FOPRIM) gas, and subsea permafrost-associated methane (SPAM), as schematically visualized in Figure 2 and described in **Paper II**.

### 3.3 Multiple methane sources contribute to methane release in the ESAS region

Three methane hotspot regions were assessed in this PhD thesis: one in the inner Laptev Sea, two in the outer Laptev Sea, and one in the East Siberian Sea. The major finding was that methane released at different methane hotspots across the ESAS showed consistently site-specific isotopic source signatures that were similar for bubble methane and dissolved methane below and above the pycnocline (Figure 4 and **Paper III**). This implies that not one but several types of methane sources cause the methane emissions across the ESAS.

#### 3.3.1 Release of microbial methane from subsea permafrost environments in the inner Laptev Sea

In the inner Laptev Sea, methane showed an isotopic fingerprint consistent with the SPAM endmember category (Figure 4 and **Paper II-III**). Furthermore, the fractional contributions of SPAM, as determined using the Bayesian MCMC algorithm, ranged from 60% to 81% (median fractions) for dissolved methane across the studied years 2016-2020 (**Paper II**), whereas it was 63% for ebullitive methane in 2020 (**Paper III**). This means that methane released at the inner Laptev Sea hotspot dominantly originates from preformed methane trapped in subsea permafrost or recent microbial production in thawed subsea permafrost. Primarily due to the observation of dense, localized ebullition and incubation-based microbial methane production rates in thawed subsea permafrost<sup>34</sup>, it was concluded that most methane is released from preformed methane pools stored within the subsea permafrost system, either as free gas or methane hydrate (**Paper II**). It was hypothesized that methane is seeping upwards along existing or developing taliks (**Paper II**). As the subsea permafrost layer is thawing rapidly<sup>35</sup>, it is expected that such methane seepage will not decrease in the future, but likely increase, albeit to uncertain extents.

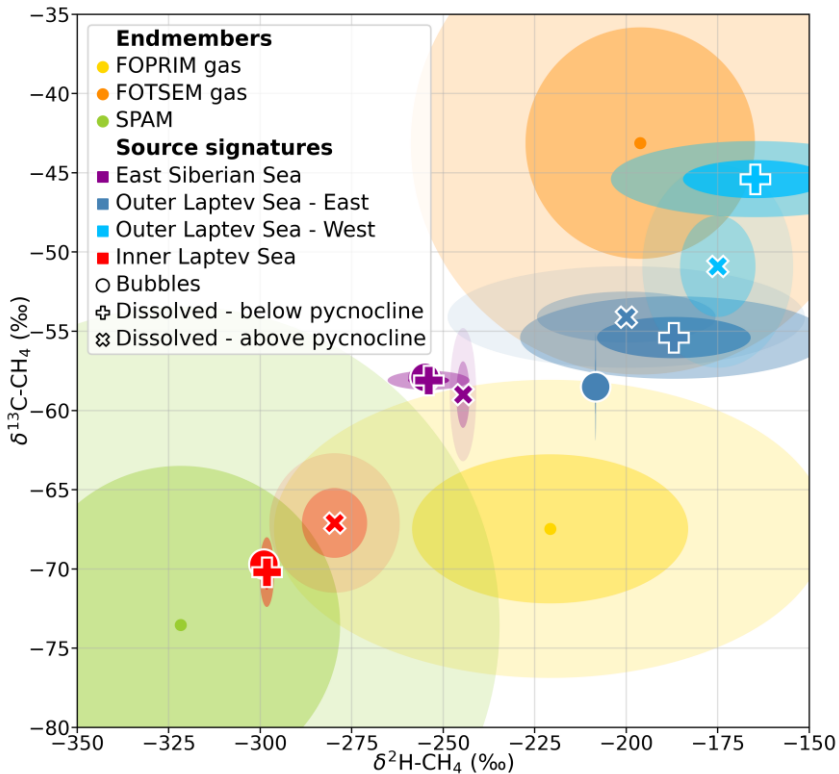


Figure 4: Methane dual-stable isotope plot showing the three considered endmembers: fossil thermogenic and secondary microbial (FOTSEM) gas, fossil primary microbial (FOPRIM) gas, and subsea permafrost-associated methane (SPAM). Furthermore, the multi-year average isotopic source signatures of bubble methane and dissolved methane below and above the pycnocline are indicated for each methane hotspot (East Siberian Sea, outer Laptev Sea – east, outer Laptev Sea – west, inner Laptev Sea). The isotopic endmembers and isotopic source signatures are indicated as mean values, 1σ, and 2σ, respectively. The figure is adapted from **Paper III**.

### 3.3.2 Seepage of fossil gas in the outer Laptev Sea and East Siberian Sea

In the outer Laptev and East Siberian Seas, the isotopic fingerprints of methane suggested dominantly seepage of different types of fossil gas at the distinct methane hotspots (Figure 4 and **Paper III**). The dual stable isotope values of methane released in the outer Laptev Sea were consistently higher than methane released in the East Siberian Sea (Figure 4), likely due to a larger contribution of thermogenic and/or secondary microbial methane to the outer Laptev Sea methane seeps (**Paper III**). At the East Siberian methane hotspot,

a larger microbial fraction in the methane mixture was deduced (**Paper III**). After applying the Bayesian MCMC algorithm, it was found that the fractional contribution of FOTSEM gas was largest at all hotspots in the outer Laptev and East Siberian Seas (**Paper III**). In the East Siberian Sea, fossil gas contributed 67% (median fraction) to both dissolved and ebullitive methane (39% FOTSEM gas, 28% FOPRIM gas). In the outer Laptev Sea, fossil gas contributed 86-95% (median fractions, 44-83% FOTSEM gas, 12-42% FOPRIM gas) to ebullitive and dissolved methane at different hotspots.

The seepage of fossil methane in the East Siberian Sea and the outer Laptev Sea corroborates the existence of fossil gas resources on the ESAS. Isotopic source apportionment can not be used to understand why these methane seepages exist. The seeps might point to methane seepage along faults from preformed fossil gas resources, a process that could remain relatively stable over the coming decades. Yet, seismic activity can be altered by climate change-induced changes in non-tectonic forces like ocean loading<sup>101–103</sup>. As fossil gas may also be trapped below/in subsea permafrost and methane hydrates, it cannot be excluded that the fossil gas is seeping from destabilizing permafrost/hydrates, a process that is expected to increase in a warming climate. The observation of fossil gas seepage yet makes it very clear that there are pools of preformed ancient methane on the ESAS that currently release methane and will do so in the future, yet at unknown rates.

### 3.4 Aerobic methane oxidation in the water column

The inner and outer Laptev Seas showed different extents of aerobic methane oxidation in the water column. While no strong indication of methane oxidation was found for the inner Laptev Sea, quantifiable amounts of methane oxidation were observed in the water column of the outer Laptev Sea.

#### 3.4.1 Inner Laptev Sea

For the inner Laptev Sea, vertical water column profiles of ~20-25 m depth showed no systematic alteration of the dual stable isotope data with water column depth at the major methane hotspot (**Paper II**). Furthermore, south of this methane hotspot, water column profiles showed a decrease in the stable hydrogen isotope values when reaching the surface, suggesting methane spreading in the surface water away from methane hotspots (**Paper II**). Moreover, when fitting linear regressions through  $\delta^{13}\text{C}_{\text{CH}_4}$  versus  $\delta^2\text{H}_{\text{CH}_4}$  data, retrieved dual stable isotope ratios,  $\Delta\delta^{13}\text{C}:\Delta\delta^2\text{H}$ , were much different from those observed for aerobic methane oxidation (**Paper II**).

### 3.4.2 Outer Laptev Sea

For the outer Laptev Sea, vertical water column profiles of ~65-70 m depth showed higher dual stable isotope values in mid/bottom waters that often decreased towards the surface water (**Paper III** and **IV**). Furthermore, further away from the methane hotspots, very high dual stable isotope values were observed that cannot be related to any methane source (**Paper IV**). Moreover, observed dual stable isotope ratios,  $\Delta\delta^{13}\text{C}:\Delta\delta^2\text{H}$ , were consistent with those observed for aerobic methane oxidation (**Paper IV**). This all points to methane oxidation in sub-pycnocline waters in the outer Laptev Sea. When using the Rayleigh equation (equation 4-5) and both  $\delta^{13}\text{C}_{\text{CH}_4}$  and  $\delta^2\text{H}_{\text{CH}_4}$  data, the fraction oxidized in samples at or below the pycnocline was estimated as 8-35% (interquartile range) using  $\delta^{13}\text{C}_{\text{CH}_4}$  data and 13-45% using  $\delta^2\text{H}_{\text{CH}_4}$  data (**Paper IV**). Importantly, this is considered a lower bound, as any dissolution from bypassing bubbles lowers the observed dual stable isotope values of dissolved methane. It can be concluded that substantial fractions of dissolved methane are oxidized in sub-pycnocline waters of the water column of the outer Laptev Sea.

## 3.5 Ebullition represents an important transport vector for methane release

For this PhD thesis, both ebullitive and dissolved methane were analyzed for methane concentration and triple-isotopic composition. It was found that ebullitive methane is an important vector for transporting methane to the water column and the atmosphere.

### 3.5.1 Ebullition: a source of methane to the water column

Methane ebullition was deduced to be an important source of methane to the water column. Firstly, the isotopic fingerprints of both ebullitive and dissolved methane were very similar at all hotspots (**Paper III**). This suggests bubble dissolution in the water column, causing the similarities in isotopic fingerprints. Secondly, the water column depths and the concentration gradients between the ebullitive and dissolved phases of methane were such that methane should partially dissolve (**Paper III**). Thirdly, observed methane concentrations in porewater were generally lower than methane concentrations observed in bottom water in the inner Laptev Sea<sup>119</sup> (**Paper II**). These concentration data do not support net diffusion of methane from the sediment into the water column as the major cause of elevated bottom-water methane concentrations. Fourthly, the dual stable isotopic composition of methane along the water column was analyzed, and the results suggested

methane dissolution from bubbles along the profile. The dual stable isotope data either remained relatively stable throughout the water column (inner Laptev Sea and East Siberian Sea) or showed an increase in dual stable isotope values in bottom/mid-water column seawater, with, in contrast, decreasing dual stable isotope values in surface water (outer Laptev Sea) (**Paper III**). Importantly, the isotopic fingerprint of methane in surface seawater was very similar to the isotopic fingerprint below the pycnocline and that of ebullitive methane (Figure 4, **Paper III**). These similarities in the isotopic fingerprints of surface-water dissolved methane and ebullitive methane, along with higher dual stable isotope values observed for dissolved methane samples deeper in the water column, suggest methane dissolution from bubbles in surface water. And if methane dissolves from rising bubbles in the surface water, it will also dissolve deeper in the water column. These four reasons strongly suggest that methane dissolves from rising bubbles in the water column. Furthermore, if there were no methane dissolution from bubbles in the water column, it is expected that observed methane concentrations in the water column would be much lower.

### 3.5.2 Ebullition: a transport pathway to the atmosphere

Methane ebullition was found to be an important process for direct methane transport towards the atmosphere. Firstly, dense ebullition patterns were observed by echosounder at methane hotspots, and in parallel, high bubble methane concentrations were found (**Paper II** and **Paper III**). Methane concentrations in bubbles were 92% (1 $\sigma$ : 7%, n=3) in bottom water and 80% (1 $\sigma$ : 22%, n=5) in surface water (**Paper III**). This means that rising bubbles contain high levels of methane, and as they travel through the shallow water columns of the ESAS, they release methane directly to the atmosphere.

Furthermore, as previously mentioned, ebullitive methane is considered an important source of methane to the dissolved methane pool in the surface water. As surface-water methane is easily transported to the atmosphere, especially by storm-induced venting<sup>67</sup>, ebullition is also inferred to be an indirect cause for methane transport towards the atmosphere (**Paper III**). Importantly, any methane transported as bubbles bypasses microbial degradation in the dissolved phase, whether in sediment porewater or the water column, thereby representing a direct transport pathway for methane transport from the seabed to the atmosphere.

## 4 Conclusions and Outlook

Methane emissions at methane hotspots across the East Siberian Arctic Shelf are dominated by old ( $^{14}\text{C}_{\text{age}} > 48000$  y BP) methane. The underlying sources of the observed ancient methane release vary across the ESAS. While microbial methane from subsea permafrost dominates methane release in the inner Laptev Sea, fossil gas seeps with different isotopic fingerprints dominate in the outer Laptev Sea and East Siberian Sea. Importantly, multiple methane sources contribute to the elevated methane observed in seawater and bubbles across the ESAS.

The multi-year isotopic fingerprints of ebullitive and dissolved methane in bottom and surface water were similar at each methane hotspot, suggesting that bubble dissolution is an important source of methane to the water column. The high concentrations of methane in surface bubbles demonstrate that methane is also directly released to the atmosphere by ebullition. Methane in the water column is, at least in sub-pycnocline waters of the outer Laptev Sea, oxidized to measurable extents, reducing the dissolved methane transport flux to the atmosphere.

Both the diversity of methane sources and the ebullitive transport pathway should be considered when estimating methane release from the ESAS region, now and in the future. There is thus a need to renew former estimates that focused on single processes. Furthermore, the results of this PhD thesis reinforce the existence of methane release from the ESAS region, even as two transport vectors, raising questions about why methane release from subsea permafrost environments is not included in global methane and Arctic carbon budgets.

There remain many knowledge gaps regarding methane release in the ESAS region. Some of these are more feasible to address in the short term than others. Follow-up studies to this PhD thesis include:

- Triple-isotopic source apportionment of methane released at the ESAS slope using methods described in **Paper I** and **Paper II**. This will expand the understanding of methane sources towards the borders of the ESAS.
- Analysis of the high-concentration bubble gas methane (**Paper III**) for doubly substituted isotopologues of methane ( $^{13}\text{CH}_3^2\text{H}$  and  $\text{CH}_2^2\text{H}_2$ ) to

possibly investigate methane formation or re-equilibration temperatures, to fine-tune the source apportionment.

- Estimation of the magnitude of ESAS-wide methane release using ESAS-wide surface water methane concentrations next to ebullition quantification. In **Paper III**, multi-year surface water methane concentrations were presented. Inter- and extrapolations of these methane concentrations, combined with meteorological data, could result in updated numbers on the diffusive methane release flux, and be compared to current estimates<sup>66,67,86,91</sup>. The high methane concentrations in surface bubbles shown in **Paper III** could, together with additional echosounder data, lead to improved estimates of the ebullitive methane flux<sup>67</sup>.
- The assessment of methane oxidation in **Paper IV** could be improved by estimating bubble dissolution rates and estimating methane oxidation assuming an open system that includes an input vector from bubble dissolution.

In addition, there are more challenging, very important data gaps that require attention to enable modeling future methane emissions from the ESAS region. One will need additional deep cores at larger distances from the coast that go through the subsea permafrost layer to identify the subsea permafrost extent and thawing rates further away from the coast. One will need data on methane concentrations at greater depths and the existence of methane hydrates for deep cores at different distances from the coast. Furthermore, it would be highly useful to measure the isotopic composition of methane in such cores to see if these values align with those observed for the released methane. Furthermore, in line with subsea permafrost thawing rates, one needs long-term data on bottom-water temperatures to determine whether these are increasing continuously and at what rates. Only with also such data could one prognose subsea permafrost stability and changes in methane release rates from the ESAS in a warming Arctic. While methane continues to be emitted from the ESAS region, which has many potential positive feedback mechanisms to climate change, greater consideration of this vulnerable region is advised.

## 5 References

1. Schaeffer, R. *et al.* Ten new insights in climate science 2024. *One Earth* **8**, 101285 (2025).
2. Intergovernmental Panel on Climate Change (IPCC). Summary for Policymakers. in *Climate Change 2022: Mitigation of Climate Change. Contribution of Working Group III to the Sixth Assessment Report of the Intergovernmental Panel on Climate Change* (eds. Shukla, P. R. *et al.*) 3–48 (Cambridge University Press, Cambridge, UK and New York, NY, USA, 2022). doi:10.1017/9781009157926.001.
3. Forster, P. *et al.* The Earth’s Energy Budget, Climate Feedbacks, and Climate Sensitivity. in *Climate Change 2021: The Physical Science Basis. Contribution of Working Group I to the Sixth Assessment Report of the Intergovernmental Panel on Climate Change* (eds. Masson-Delmotte, V. *et al.*) 923–1054 (Cambridge University Press, Cambridge, United Kingdom and New York, NY, USA, 2021).
4. Szopa, S. *et al.* Short-Lived Climate Forcers. in *Climate Change 2021: The Physical Science Basis. Contribution of Working Group I to the Sixth Assessment Report of the Intergovernmental Panel on Climate Change* (eds. Masson-Delmotte, V. *et al.*) 817–922 (Cambridge University Press, Cambridge, United Kingdom and New York, NY, USA, 2021).
5. Nisbet, E. G. *et al.* Atmospheric Methane: Comparison Between Methane’s Record in 2006–2022 and During Glacial Terminations. *Global Biogeochem. Cycles* **37**, e2023GB007875 (2023).
6. Lan, X. & Dlugokencky, E. J. Atmospheric constraints on changing Arctic CH<sub>4</sub> emissions. *Front. Environ. Sci.* **12**, (2024).
7. Saunio, M. *et al.* Global Methane Budget 2000–2020. *Earth Syst. Sci. Data* **17**, 1873–1958 (2025).
8. Schuur, E. A. G. *et al.* Climate change and the permafrost carbon feedback. *Nature* **520**, 171–179 (2015).
9. Judd, A. G., Hovland, M., Dimitrov, L. I., García Gil, S. & Jukes, V. The geological methane budget at Continental Margins and its influence on climate change. *Geofluids* **2**, 109–126 (2002).

10. Ury, E. A., Hinckley, E.-L. S., Visioni, D. & Buma, B. Managing the Global Wetland Methane-Climate Feedback: A Review of Potential Options. *Glob. Chang. Biol.* **30**, e17585 (2024).
11. Zhang, Z. *et al.* Recent intensification of wetland methane feedback. *Nat. Clim. Chang.* **13**, 430–433 (2023).
12. Comyn-Platt, E. *et al.* Carbon budgets for 1.5 and 2 °C targets lowered by natural wetland and permafrost feedbacks. *Nat. Geosci.* **11**, 568–573 (2018).
13. Rocher-Ros, G. *et al.* Global methane emissions from rivers and streams. *Nature* **621**, 530–535 (2023).
14. Schuur, E. *et al.* Permafrost and Climate Change: Carbon Cycle Feedbacks From the Warming Arctic. *Annu. Rev. Environ. Resour.* **47**, 343–371 (2022).
15. Hugelius, G. *et al.* Permafrost Region Greenhouse Gas Budgets Suggest a Weak CO<sub>2</sub> Sink and CH<sub>4</sub> and N<sub>2</sub>O Sources, But Magnitudes Differ Between Top-Down and Bottom-Up Methods. *Global Biogeochem. Cycles* **38**, e2023GB007969 (2024).
16. Knoblauch, C., Beer, C., Liebner, S., Grigoriev, M. N. & Pfeiffer, E.-M. Methane production as key to the greenhouse gas budget of thawing permafrost. *Nat. Clim. Chang.* **8**, 309–312 (2018).
17. Walter Anthony, K. *et al.* 21st-century modeled permafrost carbon emissions accelerated by abrupt thaw beneath lakes. *Nat. Commun.* **9**, 3262 (2018).
18. Turetsky, M. R. *et al.* Carbon release through abrupt permafrost thaw. *Nat. Geosci.* **13**, 138–143 (2020).
19. Sullivan, T. D. *et al.* Influence of permafrost thaw on an extreme geologic methane seep. *Permafrost. Periglac. Process.* **32**, 484–502 (2021).
20. Canadell, J. G. *et al.* Global Carbon and other Biogeochemical Cycles and Feedbacks. in *Climate Change 2021: The Physical Science Basis. Contribution of Working Group I to the Sixth Assessment Report of the Intergovernmental Panel on Climate Change* (eds. Masson-Delmotte, V. *et al.*) 673–816 (Cambridge University Press, Cambridge, United Kingdom and New York, NY, USA, 2021). doi:10.1017/9781009157896.007.
21. Lan, X. *et al.* Improved Constraints on Global Methane Emissions and Sinks Using  $\delta^{13}\text{C-CH}_4$ . *Global Biogeochem. Cycles* **35**, e2021GB007000 (2021).

22. Michel, S. E. *et al.* Rapid shift in methane carbon isotopes suggests microbial emissions drove record high atmospheric methane growth in 2020–2022. *Proceedings of the National Academy of Sciences* **121**, e2411212121 (2024).
23. Riddell-Young, B. *et al.* Microbial driver of 2006–2023 CH<sub>4</sub> growth indicated by trends in atmospheric δD–CH<sub>4</sub> and δ<sup>13</sup>C–CH<sub>4</sub>. *Proceedings of the National Academy of Sciences* **122**, e2516543122 (2025).
24. Basu, S. *et al.* Estimating emissions of methane consistent with atmospheric measurements of methane and δ<sup>13</sup>C of methane. *Atmos. Chem. Phys.* **22**, 15351–15377 (2022).
25. Ciais, P. *et al.* Why methane surged in the atmosphere during the early 2020s. *Science* **391**, eadx8262 (2026).
26. Harris, S. A. *et al.* *Glossary of Permafrost and Related Ground-Ice Terms. Technical Memorandum (National Research Council of Canada. Associate Committee on Geotechnical Research); no. ACGR-TM-142* (National Research Council of Canada, Ottawa, Ontario, 1988). doi:10.4224/20386561.
27. Van Huissteden, J. *Thawing Permafrost*. (Springer, 2020).
28. Kitover, D. C., van Balen, R. T., Vandenberghe, J., Roche, D. M. & Renssen, H. LGM Permafrost Thickness and Extent in the Northern Hemisphere derived from the Earth System Model iLOVECLIM. *Permafr. Periglac. Process.* **27**, 31–42 (2016).
29. Kitover, D., Van Balen, R., Roche, D., Vandenberghe, J. & Renssen, H. Advancement toward coupling of the VAMPER permafrost model within the Earth system model ILOVECLIM (version 1.0): Description and validation. *Geosci. Model Dev.* **8**, 1445–1460 (2015).
30. Overduin, P. *et al.* Submarine Permafrost Map in the Arctic Modeled Using 1-D Transient Heat Flux (SuPerMAP). *J. Geophys. Res. Oceans* **124**, 3490–3507 (2019).
31. Romanovskii, N., Hubberten, H.-W., Gavrillov, A. V, Tumskoy, V. E. & Kholodov, A. L. Permafrost of the east Siberian Arctic shelf and coastal lowlands. *Quat. Sci. Rev.* **23**, 1359–1369 (2004).
32. Klemann, V., Heim, B., Bauch, H. A., Wetterich, S. & Opel, T. Sea-level evolution of the Laptev Sea and the East Siberian Sea since the last glacial maximum. *Arktos* **1**, 1–8 (2015).

33. Jakobsson, M. Hypsometry and volume of the Arctic Ocean and its constituent seas. *Geochemistry, Geophysics, Geosystems* **3**, 1–18 (2002).
34. Wild, B. *et al.* Organic matter composition and greenhouse gas production of thawing subsea permafrost in the Laptev Sea. *Nat. Commun.* **13**, 5057 (2022).
35. Shakhova, N. *et al.* Current rates and mechanisms of subsea permafrost degradation in the East Siberian Arctic Shelf. *Nat. Commun.* **8**, 15872 (2017).
36. Crill, P. M. & Martens, C. S. Methane production from bicarbonate and acetate in an anoxic marine sediment. *Geochim. Cosmochim. Acta* **50**, 2089–2097 (1986).
37. Knoblauch, C., Beer, C., Sosnin, A., Wagner, D. & Pfeiffer, E.-M. Predicting long-term carbon mineralization and trace gas production from thawing permafrost of Northeast Siberia. *Glob. Chang. Biol.* **19**, 1160–1172 (2013).
38. Koch, K., Knoblauch, C. & Wagner, D. Methanogenic community composition and anaerobic carbon turnover in submarine permafrost sediments of the Siberian Laptev Sea. *Environ. Microbiol.* **11**, 657–668 (2009).
39. Wagner, D. *et al.* Methanogenic activity and biomass in Holocene permafrost deposits of the Lena Delta, Siberian Arctic and its implication for the global methane budget. *Glob. Chang. Biol.* **13**, 1089–1099 (2007).
40. Rivkina, E., Laurinavichus, K. S., Gilichinsky, D. A. & Shcherbakova, V. A. Methane Generation in Permafrost Sediments. *Doklady Biological Sciences* **383**, 179–181 (2002).
41. Rivkina, E. *et al.* Biogeochemistry of methane and methanogenic archaea in permafrost. *FEMS Microbiol. Ecol.* **61**, 1–15 (2007).
42. Natali, S. M. *et al.* Permafrost thaw and soil moisture driving CO<sub>2</sub> and CH<sub>4</sub> release from upland tundra. *J. Geophys. Res. Biogeosci.* **120**, 525–537 (2015).
43. Johnston, C. E. *et al.* Effect of permafrost thaw on CO<sub>2</sub> and CH<sub>4</sub> exchange in a western Alaska peatland chronosequence. *Environmental Research Letters* **9**, 085004 (2014).
44. Brouchkov, A. & Fukuda, M. Preliminary measurements on methane content in permafrost, Central Yakutia, and some experimental data. *Permafrost. Periglac. Process.* **13**, 187–197 (2002).

45. Rivkina, E. *et al.* Metagenomic analyses of the late Pleistocene permafrost – additional tools for reconstruction of environmental conditions. *Biogeosciences* **13**, 2207–2219 (2016).
46. Chuvilin, E., Yakushev, V. & Perlova, E. Gas and Possible Gas Hydrates in the Permafrost of Bovanenkovo Gas Field, Yamal Peninsula, West Siberia. *Polarforschung* **68**, 215–219 (1998).
47. Yakushev, V. S. & Chuvilin, E. M. Natural gas and gas hydrate accumulations within permafrost in Russia. *Cold Reg. Sci. Technol.* **31**, 189–197 (2000).
48. Cramer, B. & Franke, D. Indications for an active petroleum system in the Laptev Sea, NE Siberia. *Journal of Petroleum Geology* **28**, 369–384 (2005).
49. Gresov, A. I., Obzhurov, A. I., Yatsuk, A. V, Mazurov, A. K. & Ruban, A. S. Gas content of bottom sediments and geochemical indicators of oil and gas on the shelf of the East Siberian Sea. *Russian Journal of Pacific Geology* **11**, 308–314 (2017).
50. Kontorovich, A. E. *et al.* Geology and hydrocarbon resources of the continental shelf in Russian Arctic seas and the prospects of their development. *Russian Geology and Geophysics* **51**, 3–11 (2010).
51. Strapoć, D. Biogenic Methane. in *Encyclopedia of Geochemistry: A Comprehensive Reference Source on the Chemistry of the Earth* (ed. White, W. M.) 1–9 (Springer International Publishing, 2017). doi:10.1007/978-3-319-39193-9\_166-1.
52. Kvenvolden, K. A. Methane hydrates and global climate. *Global Biogeochem. Cycles* **2**, 221–229 (1988).
53. Kvenvolden, K. A. Gas hydrates—geological perspective and global change. *Reviews of Geophysics* **31**, 173–187 (1993).
54. Dallimore, S. & Collett, T. Intrapermafrost gas hydrates from a deep core hole in the Mackenzie Delta, Northwest Territories, Canada. *Geology* **23**, 527–530 (1995).
55. Stein, R. *et al.* Organic Carbon in Arctic Ocean Sediments: Sources, Variability, Burial, and Paleoenvironmental Significance BT - The Organic Carbon Cycle in the Arctic Ocean. in (eds. Stein, R. & MacDonald, R. W.) 169–314 (Springer Berlin Heidelberg, Berlin, Heidelberg, 2004). doi:10.1007/978-3-642-18912-8\_7.
56. Miesner, F. *et al.* Subsea permafrost organic carbon stocks are large and of dominantly low reactivity. *Sci. Rep.* **13**, 9425 (2023).

57. Shakhova, N. *et al.* Geochemical and geophysical evidence of methane release over the East Siberian Arctic Shelf. *J. Geophys. Res. Oceans* **115**, (2010).
58. Hugelius, G. *et al.* Estimated stocks of circumpolar permafrost carbon with quantified uncertainty ranges and identified data gaps. *Biogeosciences* **11**, 6573–6593 (2014).
59. Strauss, J. *et al.* 9. Permafrost. *Recarbonizing global soils—A technical manual of recommended management practices* **2**, 130 (2021).
60. Ruppel, C. Permafrost-Associated Gas Hydrate: Is It Really Approximately 1 % of the Global System? *J. Chem. Eng. Data* **60**, 429–436 (2015).
61. Obu, J. How Much of the Earth’s Surface is Underlain by Permafrost? *J. Geophys. Res. Earth Surf.* **126**, e2021JF006123 (2021).
62. MacDonald, G. J. Role of methane clathrates in past and future climates. *Clim. Change* **16**, 247–281 (1990).
63. Gautier, D. L. & Moore, T. E. *Introduction to the 2008 Circum-Arctic Resource Appraisal (CARA) Professional Paper* (U.S. Geological Survey, 2017). doi:10.3133/pp1824A.
64. Gautier, D. L. *et al.* Assessment of Undiscovered Oil and Gas in the Arctic. *Science* **324**, 1175–1179 (2009).
65. Gaedicke, C. *et al.* *BGR Energy Study 2019 - Data and Developments Concerning German and Global Energy Supplies*. (Bundesanstalt für Geowissenschaften und Rohstoffe, Hannover, 2020).
66. Shakhova, N. *et al.* Extensive methane venting to the atmosphere from sediments of the East Siberian Arctic Shelf. *Science* **327**, 1246–1250 (2010).
67. Shakhova, N. *et al.* Ebullition and storm-induced methane release from the East Siberian Arctic Shelf. *Nat. Geosci.* **7**, 64–70 (2014).
68. Weber, T., Wiseman, N. A. & Kock, A. Global ocean methane emissions dominated by shallow coastal waters. *Nat. Commun.* **10**, 4584 (2019).
69. Bange, H. W. *et al.* MEMENTO: a proposal to develop a database of marine nitrous oxide and methane measurements. *Environmental Chemistry* **6**, 195–197 (2009).
70. Kock, A. & Bange, H. W. Counting the ocean’s greenhouse gas emissions. *Eos: Earth & Space Science News* **96**, 10–13 (2015).
71. Drachev, S. S., Mazur, S., Campbell, S., Green, C. & Tishchenko, A. Crustal architecture of the East Siberian Arctic Shelf and adjacent

- Arctic Ocean constrained by seismic data and gravity modeling results. *J. Geodyn.* **119**, 123–148 (2018).
72. Svendsen, J. I. *et al.* Late Quaternary ice sheet history of northern Eurasia. *Quat. Sci. Rev.* **23**, 1229–1271 (2004).
73. Lindgren, A., Hugelius, G. & Kuhry, P. Extensive loss of past permafrost carbon but a net accumulation into present-day soils. *Nature* **560**, 219–222 (2018).
74. Ehlers, J. & Gibbard, P. L. The extent and chronology of Cenozoic Global Glaciation. *Quaternary International* **164–165**, 6–20 (2007).
75. Etiope, G., Ciotoli, G., Schwietzke, S. & Schoell, M. Gridded maps of geological methane emissions and their isotopic signature. *Earth Syst. Sci. Data* **11**, 1–22 (2019).
76. Kudo, K. *et al.* Source analysis of dissolved methane in Chukchi Sea and Bering Strait during summer–autumn of 2012 and 2013. *Mar. Chem.* **243**, 104119 (2022).
77. Kitidis, V., Upstill-Goddard, R. C. & Anderson, L. G. Methane and nitrous oxide in surface water along the North-West Passage, Arctic Ocean. *Mar. Chem.* **121**, 80–86 (2010).
78. Manning, C. C. M. *et al.* Interannual Variability in Methane and Nitrous Oxide Concentrations and Sea-Air Fluxes Across the North American Arctic Ocean (2015–2019). *Global Biogeochem. Cycles* **36**, e2021GB007185 (2022).
79. Sparrow, K. J. *et al.* Limited contribution of ancient methane to surface waters of the U.S. Beaufort Sea shelf. *Sci. Adv.* **4**, eaao4842 (2018).
80. Fenwick, L. *et al.* Methane and nitrous oxide distributions across the North American Arctic Ocean during summer, 2015. *J. Geophys. Res. Oceans* **122**, 390–412 (2017).
81. Lorenson, T. D., Greinert, J. & Coffin, R. B. Dissolved methane in the Beaufort Sea and the Arctic Ocean, 1992–2009; sources and atmospheric flux. *Limnol. Oceanogr.* **61**, S300–S323 (2016).
82. Ferré, B. *et al.* Reduced methane seepage from Arctic sediments during cold bottom-water conditions. *Nat. Geosci.* **13**, 144–148 (2020).
83. Vetrov, A. A., Lobus, N. V, Drozdova, A. N., Belyaev, N. A. & Romankevich, E. A. Methane in Water and Bottom Sediments in Three Sections in the Kara and Laptev Seas. *Oceanology* **58**, 198–204 (2018).

84. Steinbach, J. *et al.* Source apportionment of methane escaping the subsea permafrost system in the outer Eurasian Arctic Shelf. *Proceedings of the National Academy of Sciences* **118**, e2019672118 (2021).
85. Portnov, A. *et al.* Offshore permafrost decay and massive seabed methane escape in water depths >20 m at the South Kara Sea shelf. *Geophys. Res. Lett.* **40**, 3962–3967 (2013).
86. Thornton, B. F., Geibel, M. C., Crill, P. M., Humborg, C. & Mörth, C.-M. Methane fluxes from the sea to the atmosphere across the Siberian shelf seas. *Geophys. Res. Lett.* **43**, 5869–5877 (2016).
87. Kosmach, D. A. *et al.* Methane in the surface waters of Northern Eurasian marginal seas. *Doklady Chemistry* **465**, 281–285 (2015).
88. Silyakova, A. *et al.* Methane release from open leads and new ice following an Arctic winter storm event. *Polar Sci.* **33**, 100874 (2022).
89. Pohlman, J. W. *et al.* Enhanced CO<sub>2</sub> uptake at a shallow Arctic Ocean seep field overwhelms the positive warming potential of emitted methane. *Proceedings of the National Academy of Sciences* **114**, 5355–5360 (2017).
90. Shakhova, N., Semiletov, I. & Chuvilin, E. Understanding the permafrost–hydrate system and associated methane releases in the east siberian arctic shelf. *Geosciences* **9**, (2019).
91. Thornton, B. F. *et al.* Shipborne eddy covariance observations of methane fluxes constrain Arctic sea emissions. *Sci. Adv.* **6**, eaay7934 (2020).
92. Vonk, J. E. *et al.* The land–ocean Arctic carbon cycle. *Nat. Rev. Earth Environ.* **6**, 86–105 (2025).
93. Zhou, W., Leung, L. R. & Lu, J. Steady threefold Arctic amplification of externally forced warming masked by natural variability. *Nat. Geosci.* **17**, 508–515 (2024).
94. Rantanen, M. *et al.* The Arctic has warmed nearly four times faster than the globe since 1979. *Commun. Earth Environ.* **3**, 168 (2022).
95. Nicolsky, D. *et al.* Modeling sub-sea permafrost in the East Siberian Arctic Shelf: The Laptev Sea region. *J. Geophys. Res. Earth Surf.* **117**, (2012).
96. Vonk, J. E. *et al.* Activation of old carbon by erosion of coastal and subsea permafrost in Arctic Siberia. *Nature* **489**, 137–140 (2012).

97. Shakhova, N. & Semiletov, I. Methane release and coastal environment in the East Siberian Arctic shelf. *Journal of Marine Systems* **66**, 227–243 (2007).
98. Semiletov, I. P. *et al.* Carbon transport by the Lena River from its headwaters to the Arctic Ocean, with emphasis on fluvial input of terrestrial particulate organic carbon vs. carbon transport by coastal erosion. *Biogeosciences* **8**, 2407–2426 (2011).
99. Bussmann, I. Distribution of methane in the Lena Delta and Buor-Khaya Bay, Russia. *Biogeosciences* **10**, 4641–4652 (2013).
100. Bogoyavlensky, V., Kishankov, A., Kazanin, A. & Kazanin, G. Distribution of permafrost and gas hydrates in relation to intensive gas emission in the central part of the Laptev Sea (Russian Arctic). *Mar. Pet. Geol.* **138**, 105527 (2022).
101. Cai, Y. & Mouyen, M. Loading-induced stress variation on active faults and seismicity modulation in the Kuril Islands-Japan region. *Earth Planet. Sci. Lett.* **643**, 118904 (2024).
102. Luttrell, K. & Sandwell, D. Ocean loading effects on stress at near shore plate boundary fault systems. *J. Geophys. Res. Solid Earth* **115**, (2010).
103. Bohnhoff, M., Martínez-Garzón, P. & Ben-Zion, Y. Global warming will increase earthquake hazards through rising sea levels and cascading effects. *Seismological Research Letters* **95**, 2571–2576 (2024).
104. Rusakov, V. Y. & Likholat, V. V. ‘Device for underwater sampling of gas bubbles’ RU 185214 U1 G01N 1/22 (2006.01). (2018).
105. Rice, A., Gotoh, A., Ajie, H. & Tyler, S. High-precision continuous-flow measurement of delta13C and deltaD of atmospheric CH4. *Anal. Chem.* **73**, 4104–4110 (2001).
106. Sherwood, O. A., Schwietzke, S. & Lan, X. Global d13C CH4 source signature inventory 2020. *Database* (2020) doi:10.15138/qn55-e011.
107. Milkov, A. V & Etiope, G. Revised genetic diagrams for natural gases based on a global dataset of >20,000 samples. *Org. Geochem.* **125**, 109–120 (2018).
108. Andersson, A. *et al.* Regionally-Varying Combustion Sources of the January 2013 Severe Haze Events over Eastern China. *Environ. Sci. Technol.* **49**, 2038–2043 (2015).
109. Bosch, C. *et al.* Source Apportionment of Polycyclic Aromatic Hydrocarbons in Central European Soils with Compound-Specific Triple Isotopes ( $\delta^{13}\text{C}$ ,  $\Delta^{14}\text{C}$ , and  $\delta^2\text{H}$ ). *Environ. Sci. Technol.* **49**, 7657–7665 (2015).

110. Møller, J. *Spatial Statistics and Computational Methods*. (Springer-Verlag New York, 2003).
111. Roberts, G. O., Gelman, A. & Gilks, W. R. Weak convergence and optimal scaling of random walk Metropolis algorithms. *The Annals of Applied Probability* **7**, 110–120 (1997).
112. Criss, R. E. Stable Isotope Distribution. in *Global Earth Physics* 292–307 (1995). doi:<https://doi.org/10.1029/RFO01p0292>.
113. Li, J. *et al.* The evolution of multiply substituted isotopologues of methane during microbial aerobic oxidation. *Geochim. Cosmochim. Acta* **381**, 223–238 (2024).
114. Leonte, M. *et al.* Rapid rates of aerobic methane oxidation at the feather edge of gas hydrate stability in the waters of Hudson Canyon, US Atlantic Margin. *Geochim. Cosmochim. Acta* **204**, 375–387 (2017).
115. Pohlman, J. W. *et al.* Sample distillation/graphitization system for carbon pool analysis by accelerator mass spectrometry (AMS). *Nucl. Instrum. Methods Phys. Res. B* **172**, 428–433 (2000).
116. Garnett, M. H., Gulliver, P. & Billett, M. F. A rapid method to collect methane from peatland streams for radiocarbon analysis. *Ecology* **9**, 113–121 (2016).
117. Sparrow, K. J. & Kessler, J. D. Efficient collection and preparation of methane from low concentration waters for natural abundance radiocarbon analysis. *Limnol. Oceanogr. Methods* **15**, 601–617 (2017).
118. Kessler, J. D. & Reeburgh, W. S. Preparation of natural methane samples for stable isotope and radiocarbon analysis. *Limnol. Oceanogr. Methods* **3**, 408–418 (2005).
119. Purgina, D. *et al.* Iron and nitrate-driven anaerobic methane oxidation in methane seep sediments of the Laptev Sea. *Chem. Geol.* **699**, 123170 (2026).

# Acknowledgements

The last 5.5 years have been a special period of my life: focusing on one education project for so long while living in a city I gradually fell in love with. Many people have made this period a special experience.

First, I would like to thank my supervisors. We made it to the end! Örjan, I am grateful you convinced me to come to Stockholm, for the lessons on writing and rhetoric, for being passionate about climate science, for your non-breakable optimism and belief, and for showing that one can make the seemingly impossible possible! Henry, I am so happy to have gotten to know you while working with you; I have happy memories of being together in the lab, seeing whether we would create liquid oxygen or not, discussing data quality, and you spreading a reassuring atmosphere in any situation. Birgit, I am grateful for your realism and straightforwardness, your quick-thinking brain when discussing science, your critical voice, and your pragmatic attitude. Thank you, you three heroes!

Next, I would like to thank all my colleagues of the past and the present. I love the open and helpful atmosphere in our corridor, where anyone can be themselves. And: always keep up the fika! A few colleagues I would like to mention and thank specifically: Gala, you were a really great force in the lab, and I am so happy you made such a good structure when working together. Fangping, thank you for your hard work and for always being so kind in any situation. Joakim, you mean so much; I am so grateful for all the discussions we had on any topic during my PhD and for all I still learn from you.

There are many friends who made this time in Stockholm very enjoyable and allowed me to reflect on the PhD project, discuss it, and see it from different angles. Thank you all, fellow musicians, for the many occasions over the past years, including KTHAK, Orkestern Filialen, ensembles (much) further north, south, and west of Stockholm, and in different cities in the Netherlands. Also, I loved and got refreshed by all kinds of outdoor activities, with friends gathered from work, music, rowing, Swedish courses, and past and current living areas. To all my friends, here and abroad, thank you so much for spending time together!

To my dear Krebber and Brussee family: I am so grateful to have such a large and diverse family on both sides that gives so much warmth, support, and inspiration. My dear parents, Agnes and Wim, thank you for stimulating

me to grow and explore so many kinds of interests, and for raising me without a car; this might have been the first seed for a PhD on greenhouse gases! My dear brother, Ottomar, thank you for being so realistic and showing the 100% opposite works as well. My dearest Adrian, how fortunate it is that we met each other after three years of PhD life at the waste bins. Let's continue caring for our surrounding world!

Marenka Brussee

Stockholm, 2026